Antiprotonic Helium

J. Révai

(RMKI KFKI, Budapest, Hungary)

$\bar{p}$ He$^+$ Atomcule
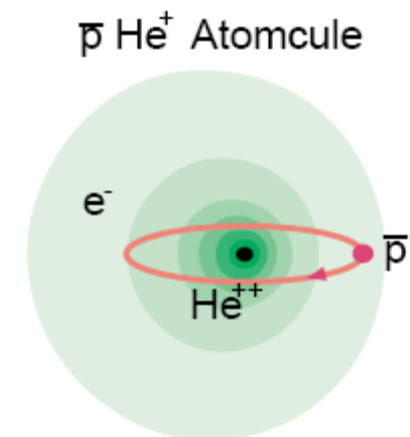
History

Exotic atoms

$$A + X^- \rightarrow (A^+ X^-)_{nl} + e^-$$

$$X : \mu^-, \pi^-, K^-, \Sigma^-, ..., \bar{p}$$

(n,l) highly excited

De-excitation mechanisms:
- Quenching
- Auger emission (internal, external)
- Decay of X
- Special case: Stark mixing

The speed of all these modes was measured and calculated and it is of the order of *ns* (10^{-9} *s*) for all kinds of atoms, light and heavy.

Anomalies for *He*:

- First in bubble chambers K^- and π^- – more particles reached the rest stage, than expected

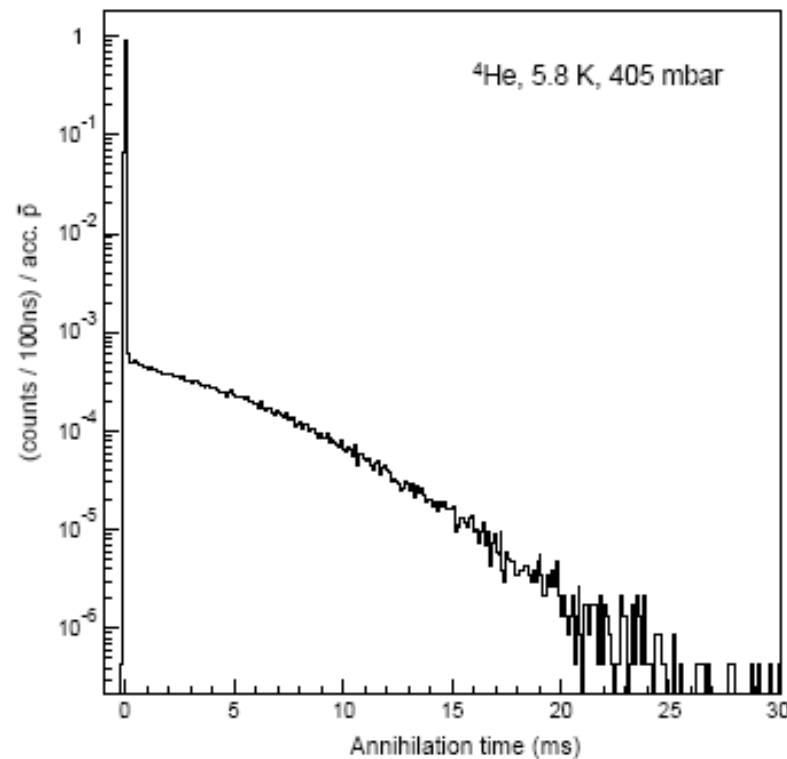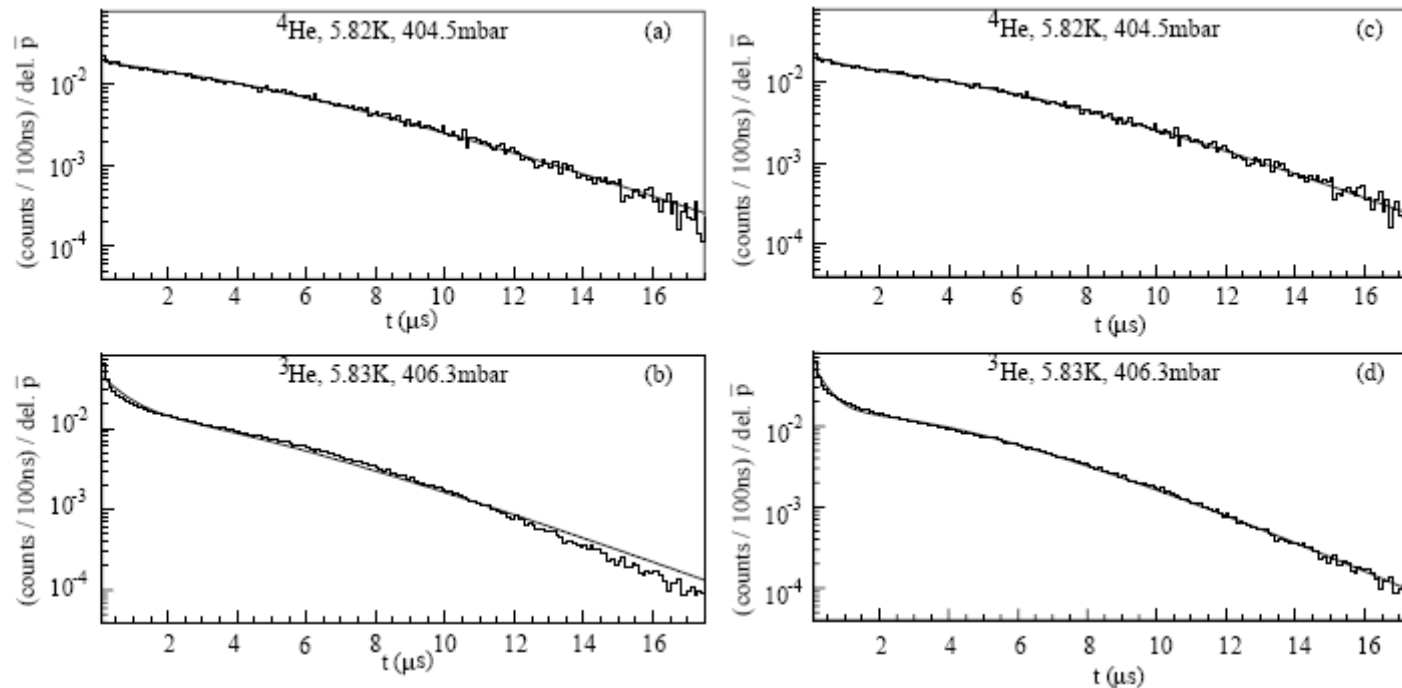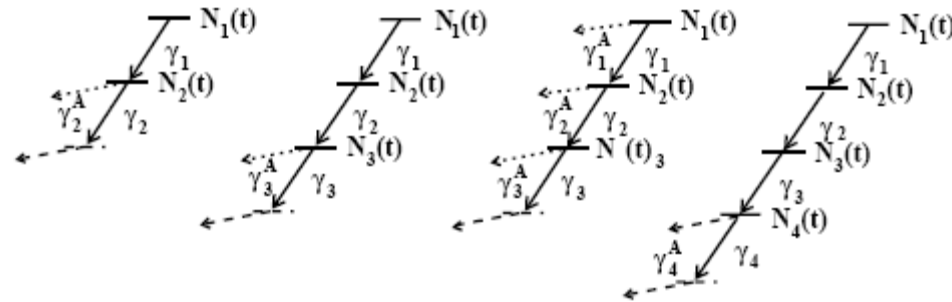- Experiments with   : DATS (Delayed Annihilation Time Spectra)
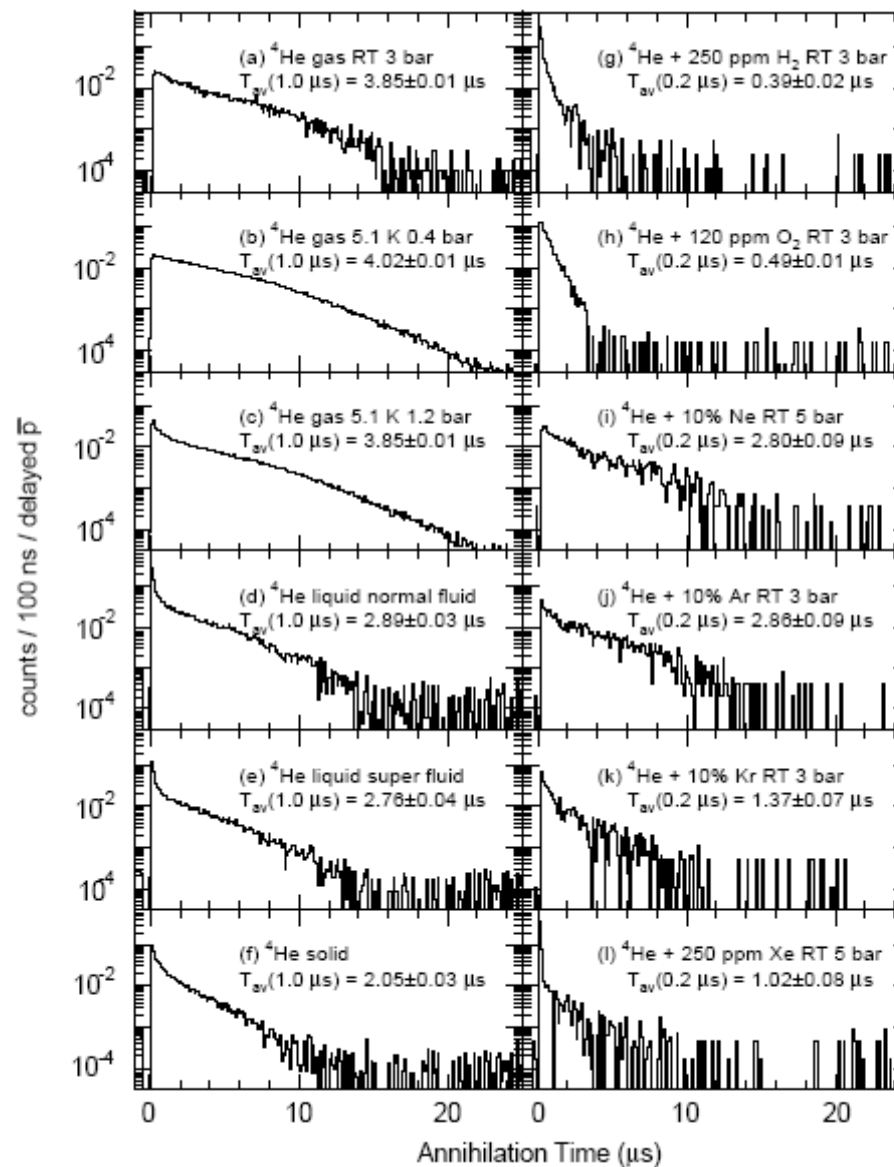

Fig. 9. Semi-logarithmic plot of a typical DATS obtained in slow extraction from LEAR with the setup shown in Fig. 7. Due to the pile-up rejection, almost no arbitrary delayed events are observed at $t > 30\ \mu s$.

Many DATS taken under different circumstances and the main conclusions from them are:

- Prompt peak plus delayed events with $\sim \mu s$ life time
- Not a single exponent

- Density and temperature independence in a wide range

(a) ^{4}He gas RT 3 bar
T_{av}(1.0 μs) = 3.85±0.01 μs

(b) ^{4}He gas 5.1 K 0.4 bar
T_{av}(1.0 μs) = 4.02±0.01 μs

(c) ^{4}He gas 5.1 K 1.2 bar
T_{av}(1.0 μs) = 3.85±0.01 μs

(d) ^{4}He liquid normal fluid
T_{av}(1.0 μs) = 2.89±0.03 μs

(e) ^{4}He liquid super fluid
T_{av}(1.0 μs) = 2.76±0.04 μs

(f) ^{4}He solid
T_{av}(1.0 μs) = 2.05±0.03 μs

(g) ^{4}He + 250 ppm H_2 RT 3 bar
T_{av}(0.2 μs) = 0.39±0.02 μs

(h) ^{4}He + 120 ppm O_2 RT 3 bar
T_{av}(0.2 μs) = 0.49±0.01 μs

(i) ^{4}He + 10% Ne RT 5 bar
T_{av}(0.2 μs) = 2.80±0.09 μs

(j) ^{4}He + 10% Ar RT 3 bar
T_{av}(0.2 μs) = 2.86±0.09 μs

(k) ^{4}He + 10% Kr RT 3 bar
T_{av}(0.2 μs) = 1.37±0.07 μs

(l) ^{4}He + 250 ppm Xe RT 5 bar
T_{av}(0.2 μs) = 1.02±0.08 μs

counts / 100 ns / delayed $\bar{p}$

Annihilation Time (μs)

- ~3% of all events
- Isotope effect ^{3}He -^{4}He

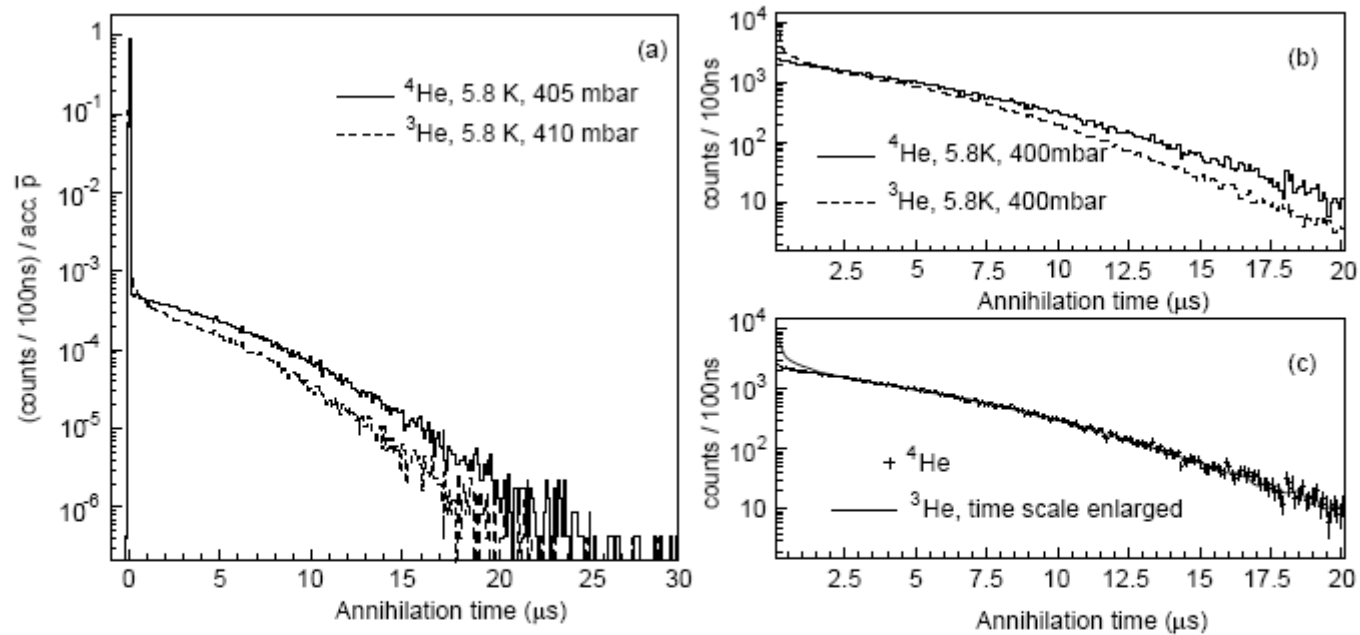
Fig. 16. (a) Comparison of typical DATS of ^{3}He and ^{4}He at same conditions. (b) Enlarged part of (a) showing only the delayed components. (c) Same spectra as in (a), with the time scale of the ^{3}He spectrum enlarged by 14.6% (solid line). The error bars of the ^{4}He spectrum include those of both spectra. From [16].
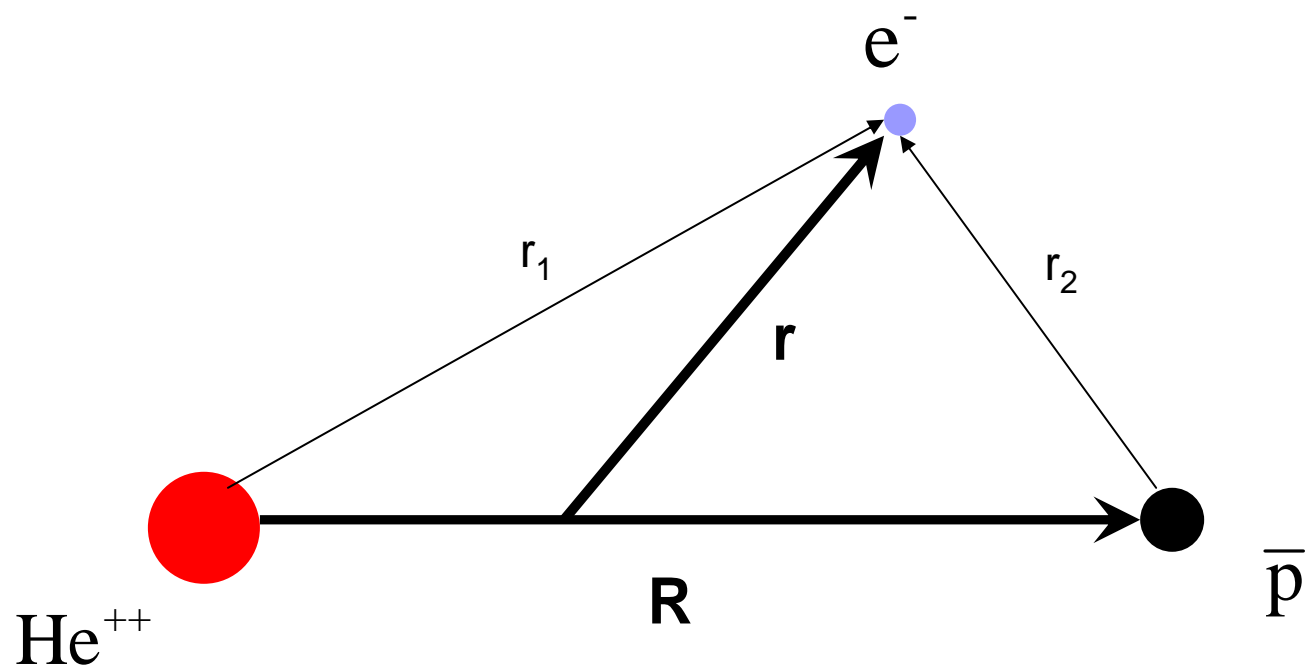
- Effect of foreign atom contamination: noble gases, H_2 , O_2: density dependent decrease of life time

Overall conclusion from DATS:

three-body objects stable against Auger-emission and collisional quenching

Early theory

$$\hat{H} = -\frac{1}{2\mu_1}\Delta_{\vec{r}} - \frac{1}{2\mu_2}\Delta_{\vec{R}} - \frac{2}{r_1} + \frac{1}{r_2} - \frac{2}{R}$$

$$\vec{r}_1 = \frac{m_{\bar{p}}}{m_{He} + m_{\bar{p}}}\vec{R} + \vec{r}, \quad \vec{r}_2 = -\frac{m_{He}}{m_{He} + m_{\bar{p}}}\vec{R} + \vec{r}$$

$$\xi = \frac{r_1 + r_2}{R}, \quad \eta = \frac{r_1 - r_2}{R} \quad \text{spheroidal coordinates}$$

$$m_{^4He} = 7294.296, \; m_{^3He} = 5495.885, \; m_{\bar{p}} = 1836.1527$$
$$\text{in units of } m_e.$$

Energy unit 1 a.u.$=27.2$ eV

$$\hat{H}\Psi_{NL}(\vec{r},\vec{R}) = E_{NL}\Psi_{NL}(\vec{r},\vec{R})$$

NL – atomic orbit notation

Jv – molecular notation, *J=L*, v=N-L-1

Series of attempts

- Exotic atom

$$He \Rightarrow \ \mathrm{E}_{\mathrm{I}_1} = 0.904 \ \text{a.u.}, \ \mathrm{E}_{\mathrm{I}_2} = \frac{1}{2}Z^2 = 2 \ \text{a.u.}$$

$$\mathrm{E}_{He} = -2.904 \ \text{a.u.}$$

$$\Psi_{He} \sim \varphi_{1s}(r_1)\varphi_{1s}(r_2) \qquad\qquad Z_{eff}$$

$$-2.094 = -2 \cdot Z_{eff}^2 \ \frac{1}{2\,\mathrm{n}^2} \quad \mathrm{n}{=}1$$

$$Z_{eff} = 1.7 \ (<2, \text{ imitating the e-e repulsion})$$

$$\Psi_{(He,\bar{p},e)} = \varphi_{1s}(r_1)\varphi_{NL}(R)$$

$\varphi_{NL} - $ hydrogenic function in Z_{eff} in such a way

$$-\frac{1}{2}Z_{eff}^2 = -\frac{\mu}{2N^2}Z_{eff}^2$$

$$N \sim \sqrt{\mu} \sim 38$$

level spacings, el.m. transition rates

etc. - orders of magnitude

- Configuration mixing

$$\Psi_{Jv} \sim \sum_{nl,NL} [\varphi_{nl}(r_1)\varphi_{NL}(R)]^J c_{nl,NL}$$

Only a few terms (Ohtsuki, Yamazaki) to account for electron polarization by $\overline{p}$, more extended by Kartavtsev.

- Born-Oppenheimer (BO) approach (Shimamura)

$$\Psi_{Jv}(\vec{r},\vec{R}) \sim \varphi_{1\sigma}(\vec{r};R)\, u_{Jv}(\vec{R})$$

$$\left(-\frac{1}{2\mu_1}\Delta_{\vec{r}} - \frac{2}{r_1} + \frac{1}{r_2}\right)\varphi_{1\sigma}(\vec{r};\vec{R}) = \varepsilon_{1\sigma}(R)\,\varphi_{1\sigma}(\vec{r};R)$$

Coulombic two-center problem, exact solution in spheroidal coordinates $\vec{r} \to \xi,\eta,R$

Substituting into $H\Psi = E\Psi$ and neglecting the effect of $\Delta_{\vec{R}}$ on $\varphi_{1\sigma}$ (adiabatic or slow motion) we get for $u_{Jv}(\vec{R})$:

$$\left(-\frac{1}{2\mu_2}\Delta_{\vec{R}} - \frac{2}{R} + \varepsilon_{1\sigma}(R) \right) u_{Jv}(\vec{R}) = E_{Jv}\, u_{Jv}(\vec{R})$$

$$u_{Jv}(\vec{R}) \sim \frac{u_{Jv}(R)}{R} Y_{JM}(\hat{R})$$

$$\left(-\frac{1}{2\mu_2}\left[\frac{d^2}{dR^2} - \frac{J(J+1)}{R^2} \right] - \frac{2}{R} + \varepsilon_{1\sigma}(R) \right) u_{Jv}(R) = E_{Jv}\, u_{Jv}(R)$$
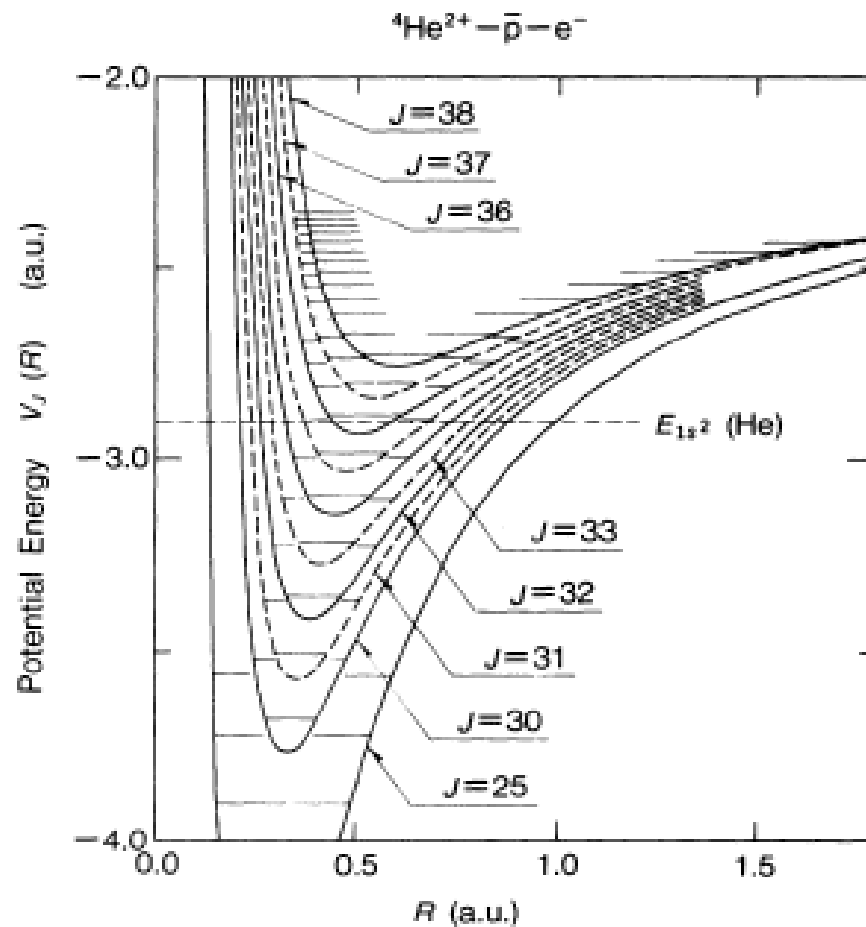
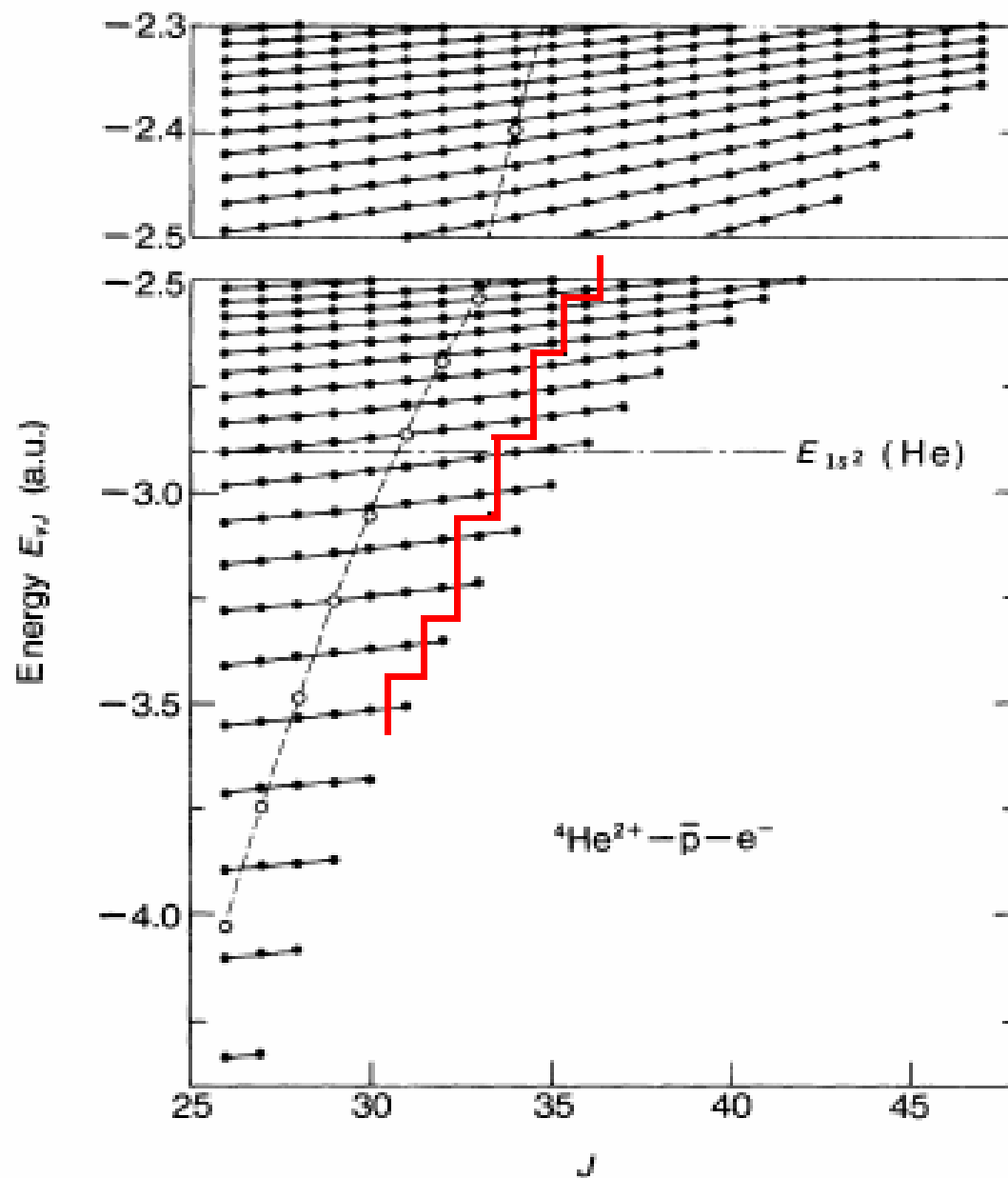FIG. 3. The effective potentials $V_J(R)$ for $J = 25$ and $J = 30$–38 for ${}^4\text{He}^{2+}$-$\bar{p}$-e^-. Some rovibrational levels supported by $V_J(R)$ are indicated by horizontal lines. The energy of the ground-state helium is also shown. The circular state closest to this energy is $(v, J) = (0, 36)$.

Energy E_ν (a.u.)

E_{1s^2} (He)

$^4He^{2+} - \bar{p} - e^-$

J
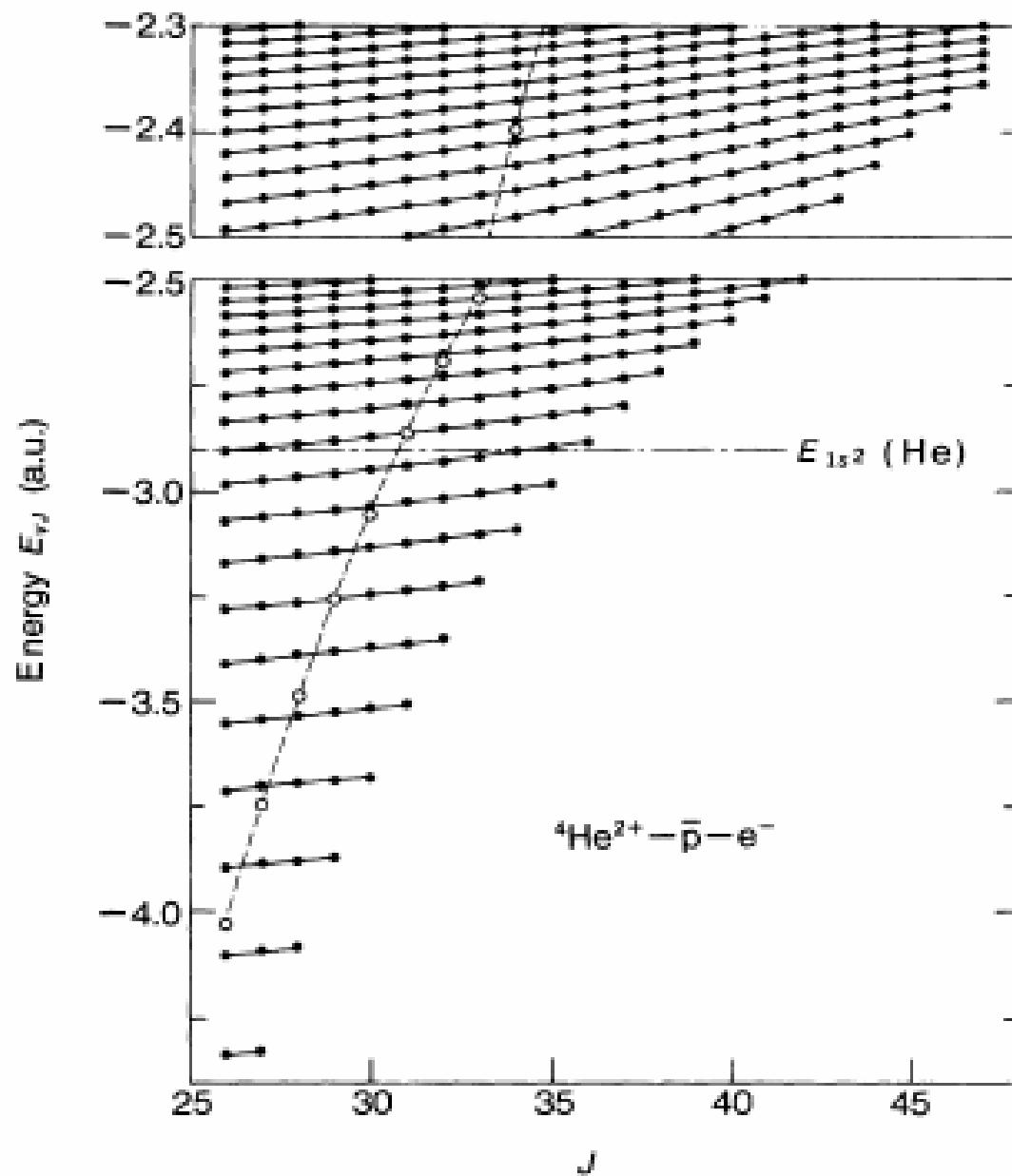
Summary of early attempts

Energy spectrum   – ~3-4 figures,
El. M. transitions   – acceptable
Auger probabilities – weak
Altogether   – good qualitative picture
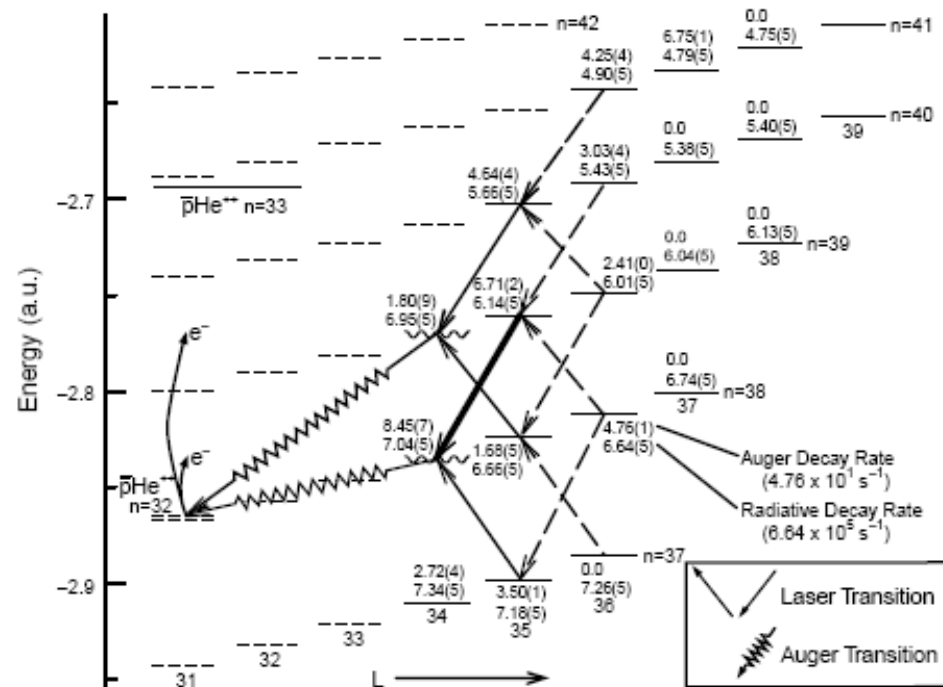   with explanation of metastability

Laser spectroscopy

Up to now no experimental information about individual levels.

Laser-induced transitions – precise measurements of level spacings.

Here the level spacings (~2 eV) is ok for tunable lasers.

Induced transitions between long-lived and short-lived states detecting the annihilation products

Since $\Delta J=1$ two type of transitions: favoured with $\Delta v=0$ and unfavoured with $\Delta v=2$
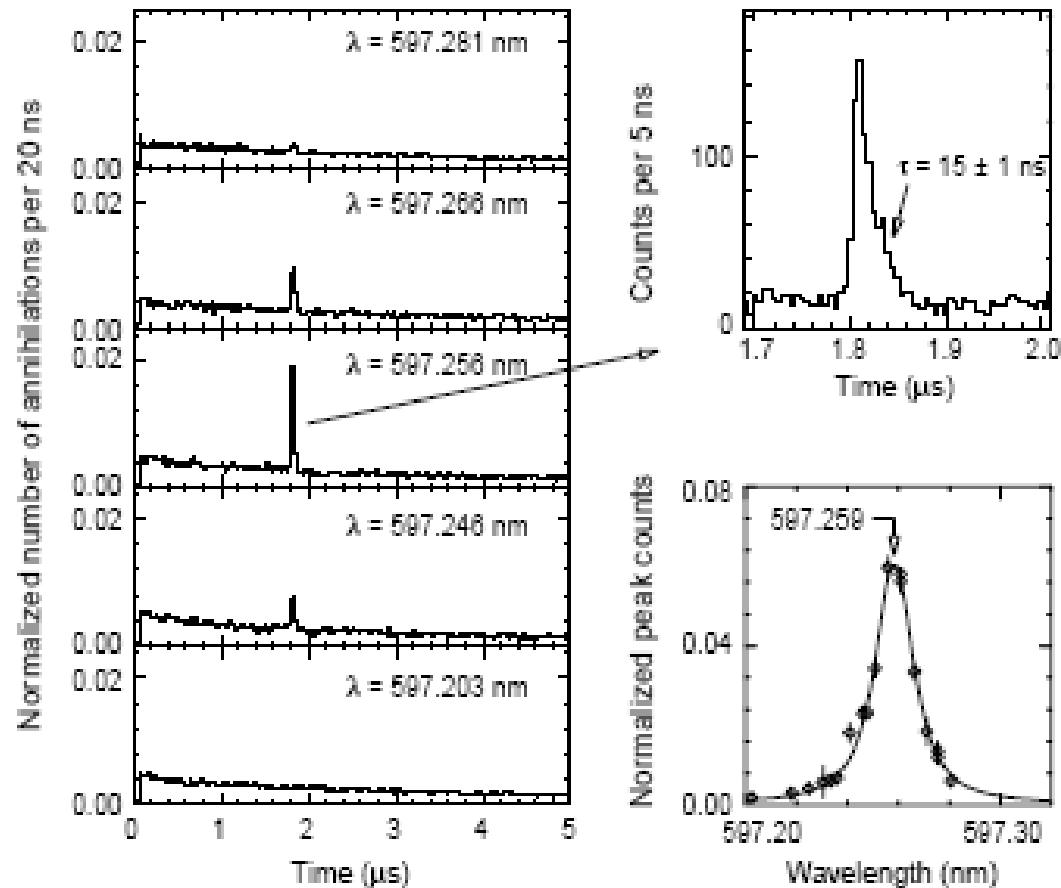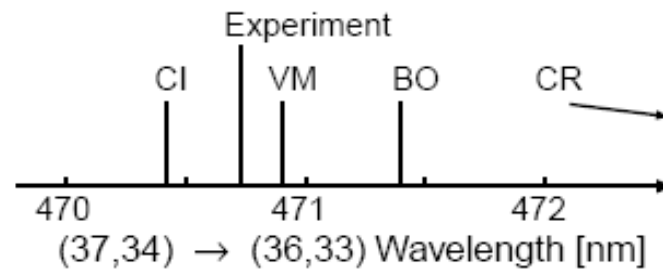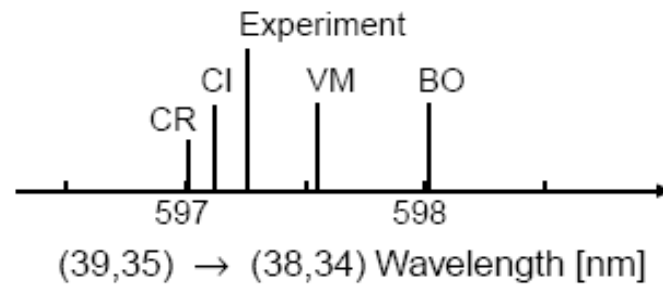
Fig. 32. First successful observation of laser resonance of antiprotonic helium, now attributed to the $(n, l) = (39, 35) \rightarrow (38, 34)$ transition. Left: Observed time spectra of delayed annihilation of antiprotons with laser irradiation of various vacuum wavelengths near 597.2 nm. Spikes due to forced annihilation through the resonance transitions are seen. Upper right: Enlarged time profile of the resonance spike. Lower right: Normalized peak count versus vacuum wavelength in the resonance region. From [29].

Precise wave length measurement of metastable – short-lived transitions

Accuracy of existing calculations clearly not enough

Experiment

CR CI VM BO

597   598

$(39,35) \rightarrow (38,34)$ Wavelength [nm]

Experiment

CI VM BO CR

470   471   472

$(37,34) \rightarrow (36,33)$ Wavelength [nm]
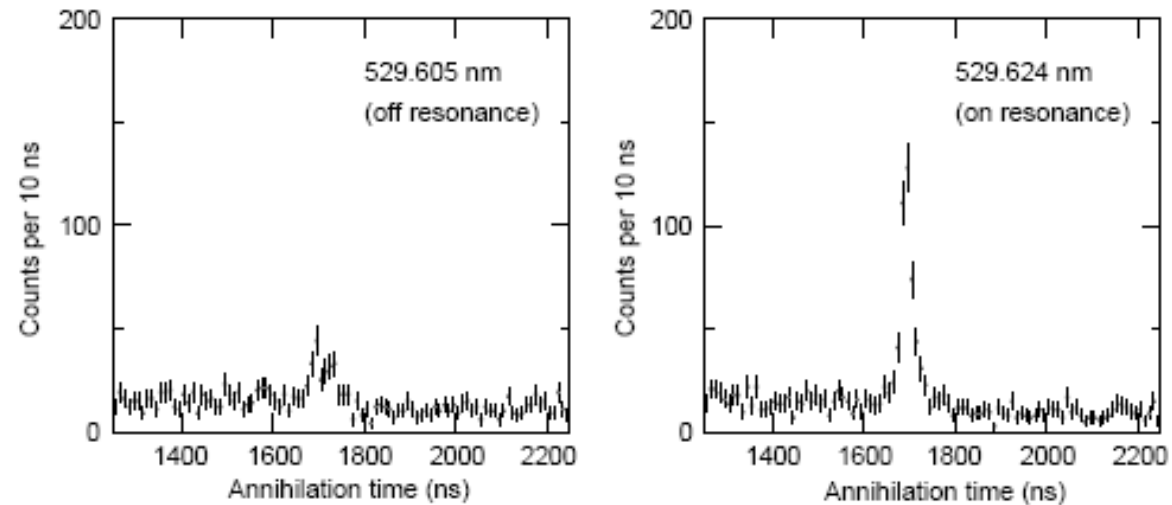
Double laser resonances

Fig. 36. Observation of the $(n, l) = (38, 35) \rightarrow (37, 34)$ transition by using the "double-resonance" method, i.e., the first laser was set to the already known 470-nm resonance [$(n, l) = (37, 34) \rightarrow (36, 33)$], while the $(38, 35) \rightarrow (37, 34)$ transition was searched for with the second laser. Left: First laser at 470.724 nm, second laser at 529.605 nm (off resonance). Right: first laser at 470.724 nm, second laser at 529.622 nm. From Ref. [34].
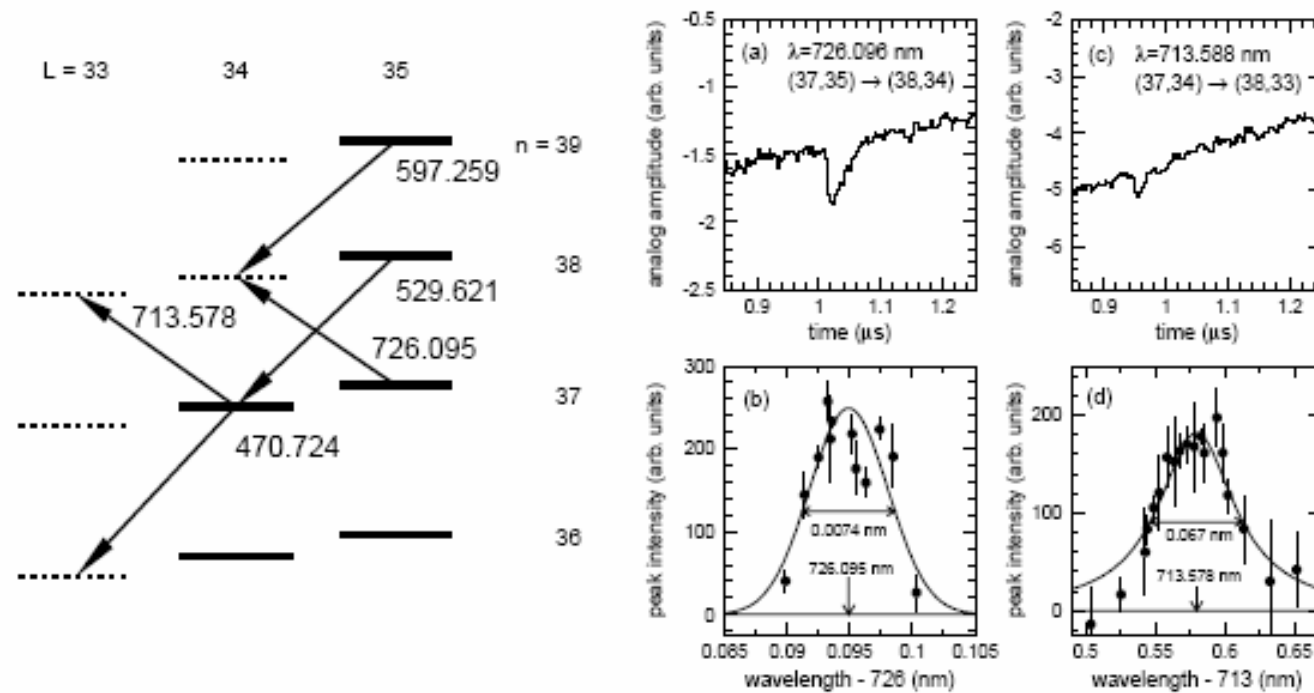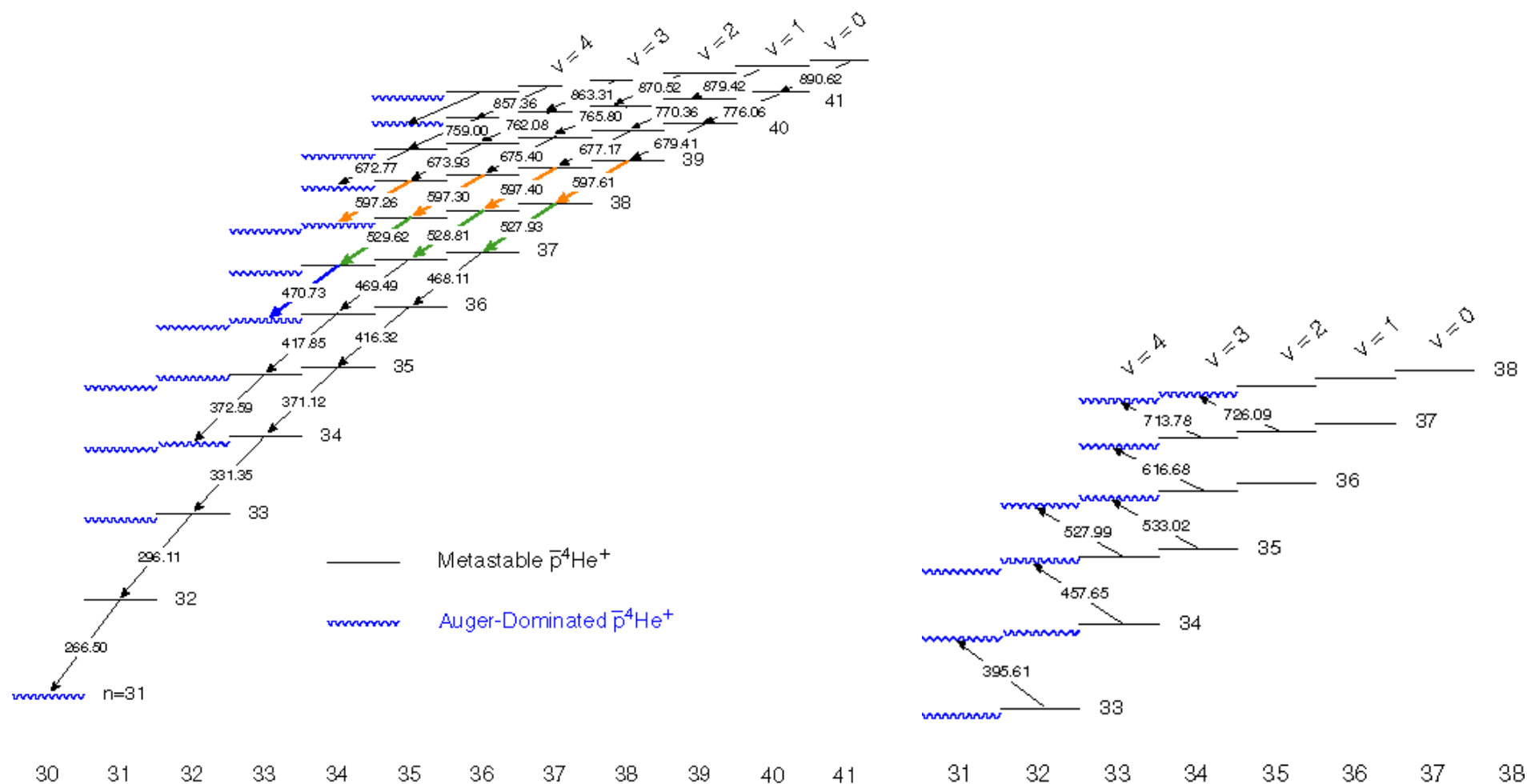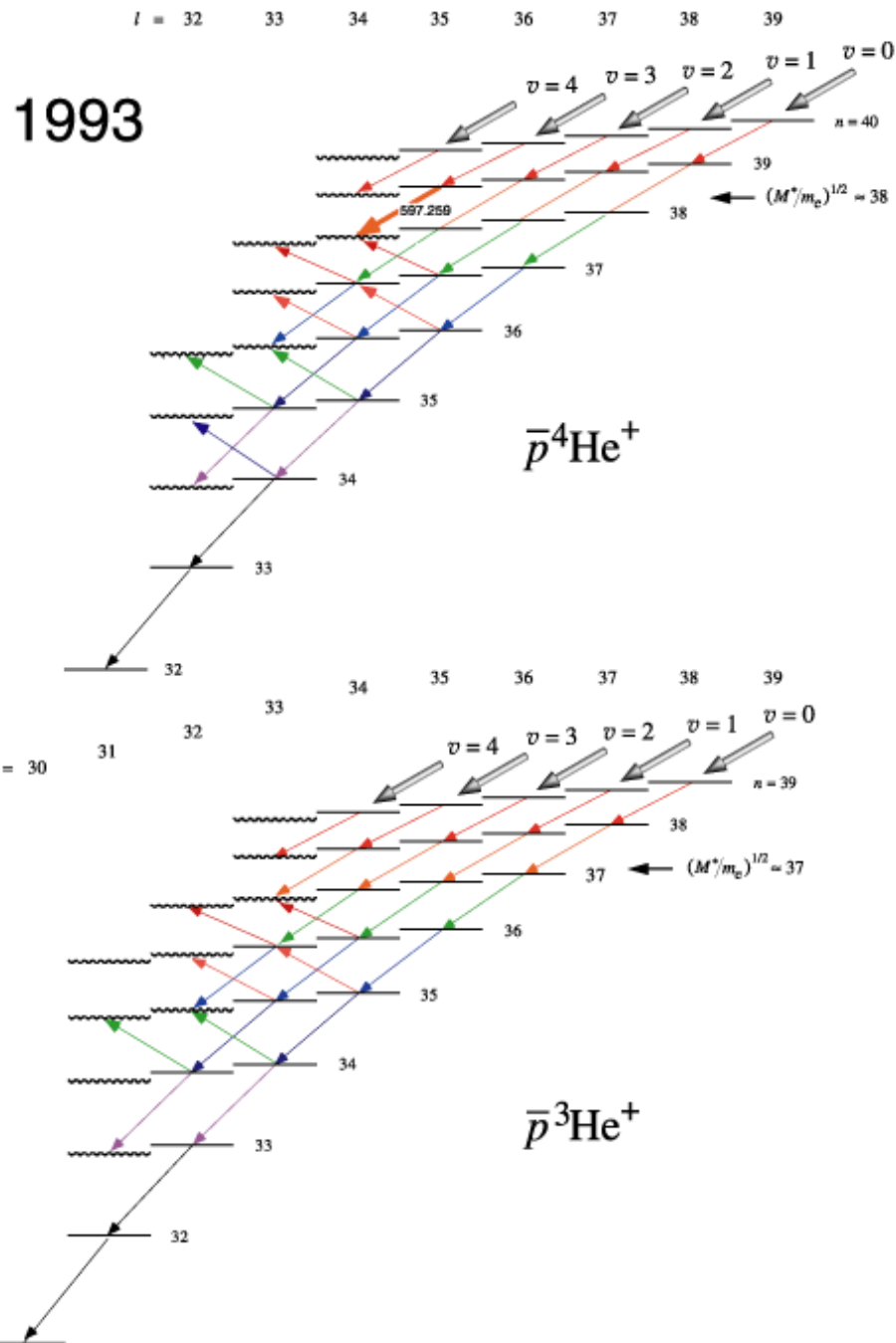
Unfavoured transitions

Fig. 37. (Left) Partial level scheme involving two unfavoured resonances of 726 and 714 nm. (Right) (a) ADATS showing a resonance spike at 726.096 nm. (b) Resonance profile of the 726 nm transition. A single Gaussian function is used to determine the central wavelength. (c) ADATS showing a resonance spike at 713.588 nm. (d) Resonance profile of the 714 nm transition. From Ref. [35].

Many transitions measured

Favoured

Unfavoured

1993

$l = 32 \quad 33 \quad 34 \quad 35 \quad 36 \quad 37 \quad 38 \quad 39$

$v = 0 \quad v = 1 \quad v = 2 \quad v = 3 \quad v = 4$

$n = 40$

39

$(M^*/m_e)^{1/2} \approx 38$

597.259

38

37

36

35

34

33

32

$\overline{p}\,{}^4\mathrm{He}^+$

$l = 30 \quad 31 \quad 32 \quad 33 \quad 34 \quad 35 \quad 36 \quad 37 \quad 38 \quad 39$

$v = 0 \quad v = 1 \quad v = 2 \quad v = 3 \quad v = 4$

$n = 39$

38

37

$(M^*/m_e)^{1/2} \approx 37$

36

35

34

33

32

$\overline{p}\,{}^3\mathrm{He}^+$

More precise theories

Extended variational calculations, high-precision, 6-8-10 figures

- Korobov-1

$$\Psi_M^J(\vec{r},\vec{R}) = \sum_m D_{Mm}^{J\lambda}(\Phi,\Theta,\varphi) F_m^{J\lambda}(r,R,\vartheta)$$

r, R, ϑ - triangle variables

$r, R, \vartheta \rightarrow r_1, r_2, R \rightarrow \xi, \eta, R$

$$F_m^{J\lambda}(\xi,\eta,R) = R^m \left[(\xi^2-1)(1-\eta^2)\right]^{\frac{m}{2}} R^{N_{sh}} \sum_n c_n R^{i_n} \xi^{j_n} \eta^{k_n} e^{-(\alpha+\beta\xi)R}$$

$N \sim 528, 880, 1728, 2364, ...$

$\Delta E \sim$ 6th figure ~ 0.001 nm

- Korobov-2

$$\Psi_M^J(\vec{r},\vec{R}) = \sum_{l_1+l_2=J} R^{l_1} r^{l_2} \left[Y_{l_1}(\hat{R}) Y_{l_2}(\hat{r}) \right]_M^J G_{l_1 l_2}^J(r,R,\vartheta)$$

$$G_{l_1 l_2}^J = \sum_i c_i e^{-\alpha_i R - \beta_i r - \gamma_i |\vec{R}-\vec{r}|}$$

$\alpha_i, \beta_i, \gamma_i$ − quasi randomly
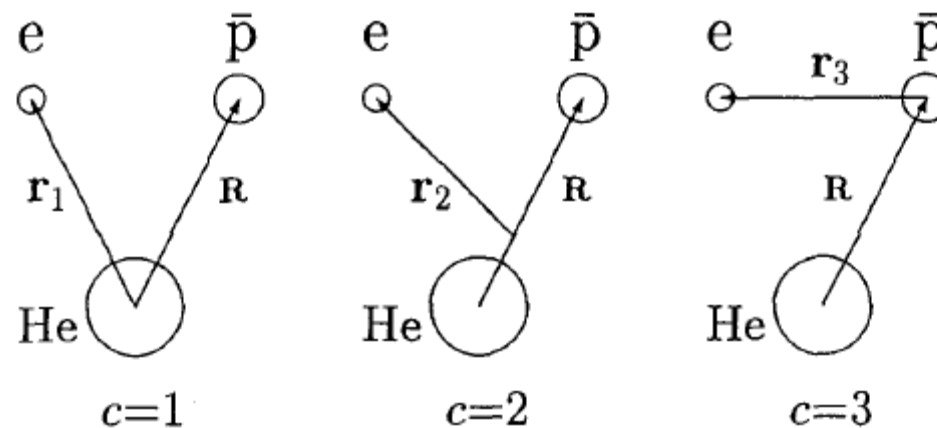
~1400 terms, tens figure in energy

- Kino, Kamimura

Fig. 1. Three rearrangement channels and coordinates adopted in this work.

$$\Psi^J_M = \sum_{c=1}^{3} \Phi^{J(c)}_M(\vec{r}_c, \vec{R})$$

$$\Phi^J_M(\vec{r}, \vec{R}) = \sum_{N,L,n,l} c_{nl,NL}\, r^l R^L e^{-\left(\frac{r}{r_n}\right)^2} e^{-\left(\frac{R}{R_n}\right)^2} \left[Y_L(\hat{R})Y_l(\hat{r})\right]^J_M$$
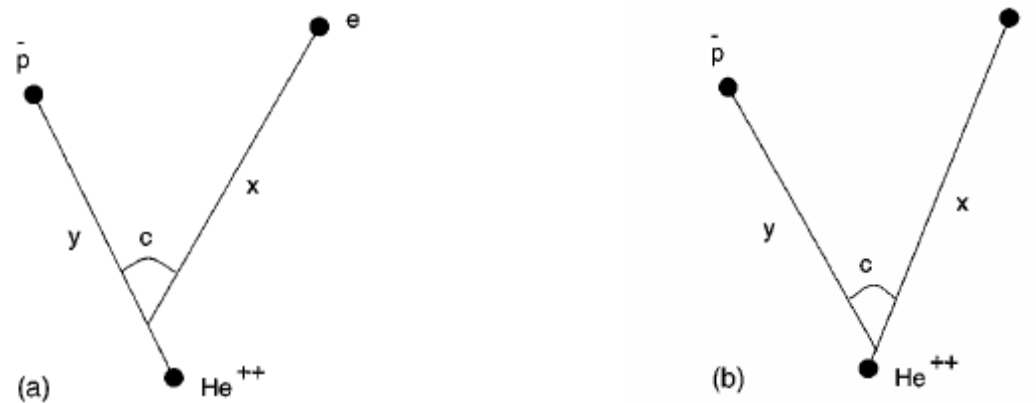
- Elander, Yarevsky

FIG. 1. Jacobi coordinate systems: (a) ''standard'' Jacobi coordinates and (b) our choice, discussed in the text. The angular variable $c = \cos\phi = (\hat{x}, \hat{y})$.

$$\Psi = \sum_m D_{Mm}^{J\lambda}(\alpha, \beta, \gamma) F_m^{J\lambda}(x, y, \phi)$$

Coupled partial differential equations for $F_m^{J\lambda}$,
Solved by tricky finite-element method on a three-dimensional grid.

Both the measurements and the calculations reached a level of accuracy when relativistic and QED corrections should be taken into account, at least to order of α^2.
Various terms:

- Electron relativistic motion (Dirac equation, Pauli approximation)

$$H_e = -\alpha^2 \frac{1}{8m^3} p^4 + \alpha^2 \left[\frac{Z_1}{8} 4\pi \delta(\mathbf{r}_{\text{He}}) + \frac{Z_2}{8} 4\pi \delta(\mathbf{r}_{\bar{p}}) \right]$$

- Other QED effects
    - mass correction
    - retardation effect
    - vacuum polarization
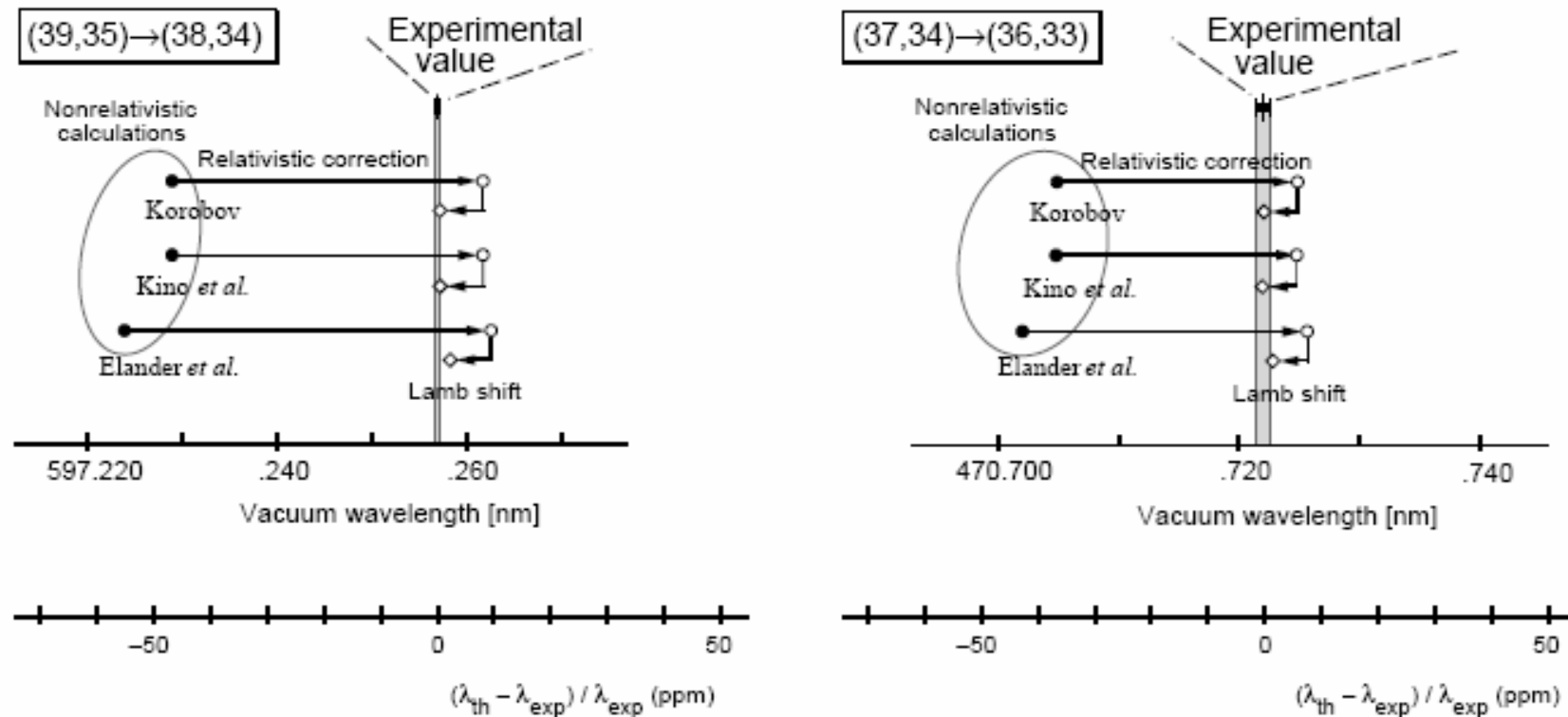   - interaction with electromagnetic vacuum

Finally

Fig. 67. Fine comparison of the wavelengths for the $(39,35) \rightarrow (38,34)$ transition at 597 nm and the $(37,34) \rightarrow (36,33)$ transition at 470 nm between the experiment and the theory. The experimental values of the vacuum wavelengths for transitions $(39,35) \rightarrow (38,34)$ and $(37,34) \rightarrow (36,33)$ are compared with recent theoretical values [22–24,26], which agree within precisions of a few ppm when the relativistic corrections and the Lamb shift are taken into account. From [38].

Further issues

<u>Experimental</u>

Lifetime and population measurements

Pressure shift and broadening

Effect of foreign molecules, especially H_2

Fine- and hyperfine splitiing

<u>Theoretical</u>

Auger emission probability

Interactions with atoms and molecules of media

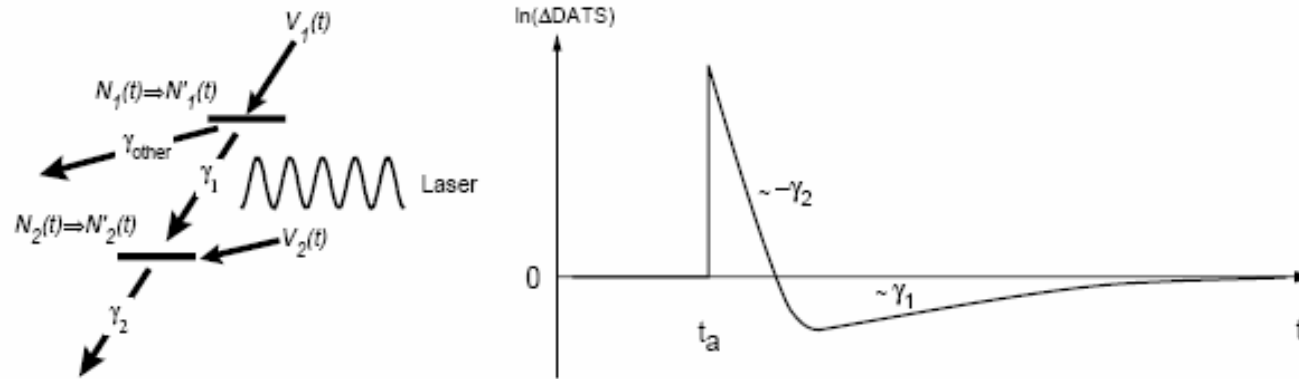Atomcule formation, initial population

- Lifetime

From peak shape

Fig. 38. Two-level laser resonance scheme (left) and a typical $\Delta(DATS)$ shape of Eq. (103) (right). From [37].

Fast decrease – Auger decay of the lower level – γ_2

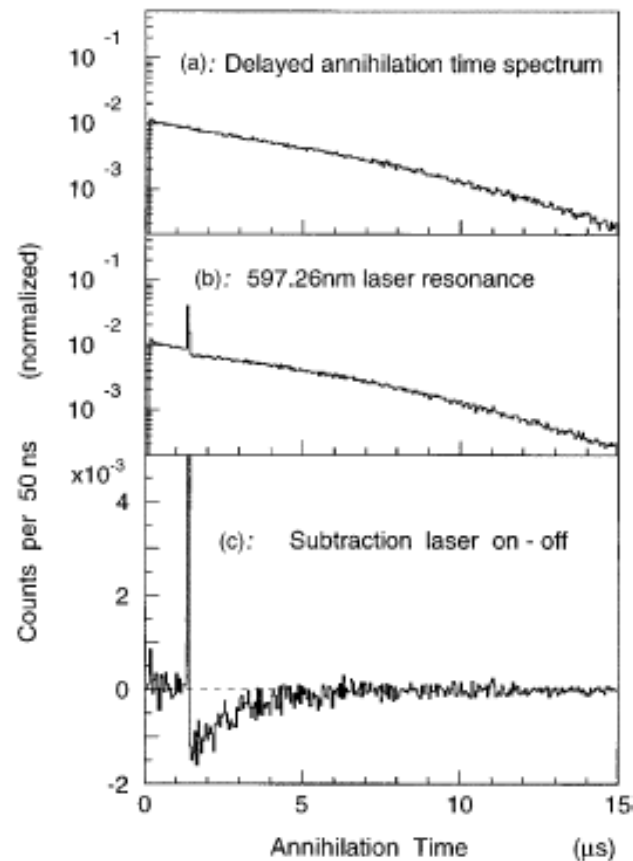Slow increase – feeding of the emptied upper level – γ_1

Fig. 41. (a) $\bar{p}He^+$ delayed annihilation time spectrum taken with ^4He gas target of 0.55 bar and 6.3 K. (b) 579.26-nm resonance induced at $t = 1.35$ ms on the time spectrum. (c) Depletion-recovery spectrum $\Delta DATS$, the difference between the two normalised spectra (a) and (b). From [37].
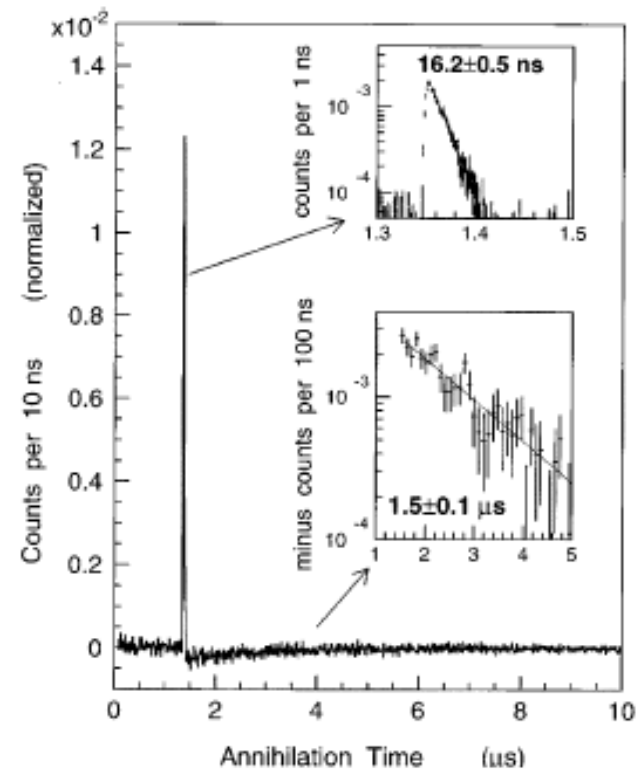
Fig. 42. Depletion-recovery spectrum of the 597 nm resonance at 0.55 bar and 6.3 K. The lifetime of the resonance parent state can be derived from the recovery rate of this spectrum. From [37].
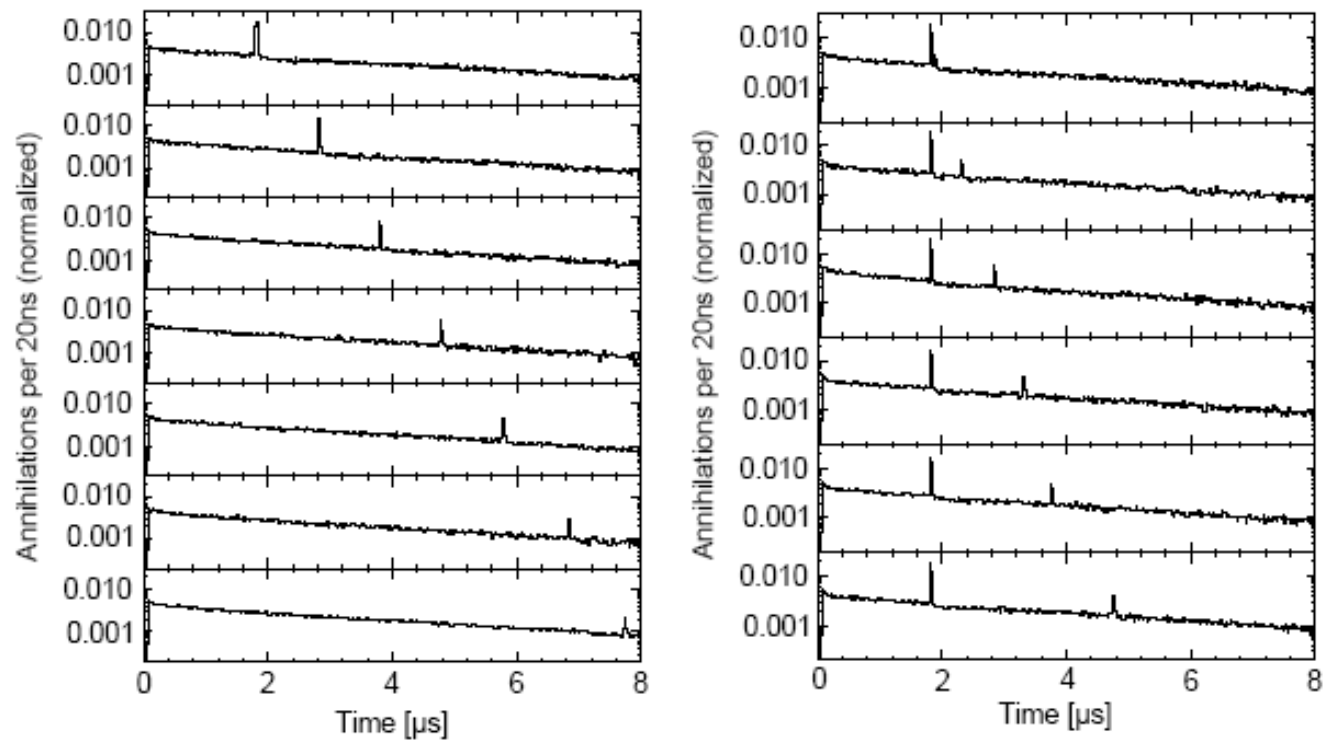
■ Peak intensities versus shooting time

Fig. 39. Antiproton annihilation time spectra (DATS) of the 597.26-nm resonance. Left: obtained by varying the laser trigger times of a single laser. Right: obtained by varying the laser trigger times of two lasers; the first laser was ignited at a fixed time $t_1 = 1.8\,\mu s$, while the second laser pulse was delayed with respect to the first by a range of values between $t_2 = t_1 + 50\,ns$ (top-right) and $t_1 + 4.0\,\mu s$ (bottom-right). From [34].

$N_{(39,35)}(t)$ – one laser

Population of upper levels feading the (39,35) – two lasers.
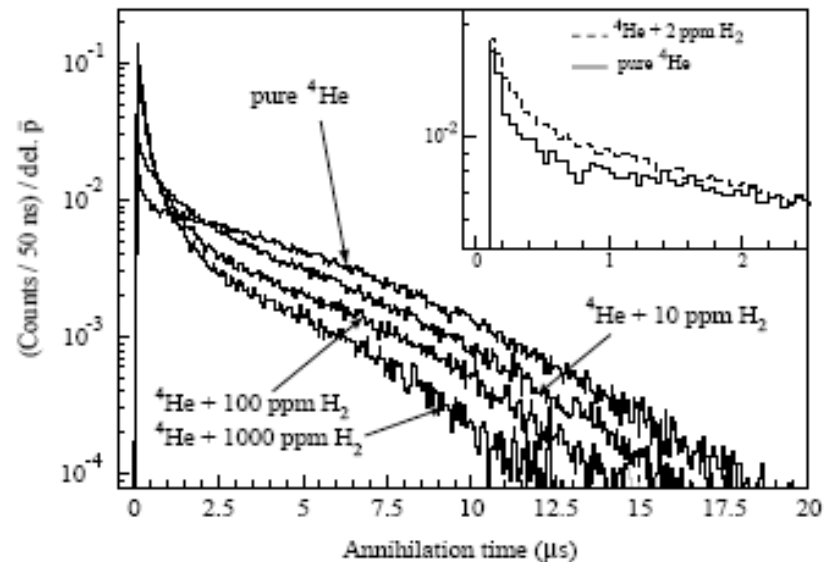
Effect of H$_2$ admixture

Fig. 52. DATS with various concentrations of H$_2$ admixtures in helium medium of 1.1 bar at 30 K. The prompt time region is removed in the data taking stage and all the spectra are normalized so as to give the same total delayed fraction. The inset compares the early time region of pure helium and 2 ppm hydrogen admixture. From [40].

Laser spectroscopy: higher levels – stronger effect of lifetime shortening,

with suitable concentration the higher level can be made shorter lived, then the lower one.

HAIR – Hydrogen Assisted Inverse Resonance

Metastable-metastable transition with the higher level made shorter lived by hydrogen contamination
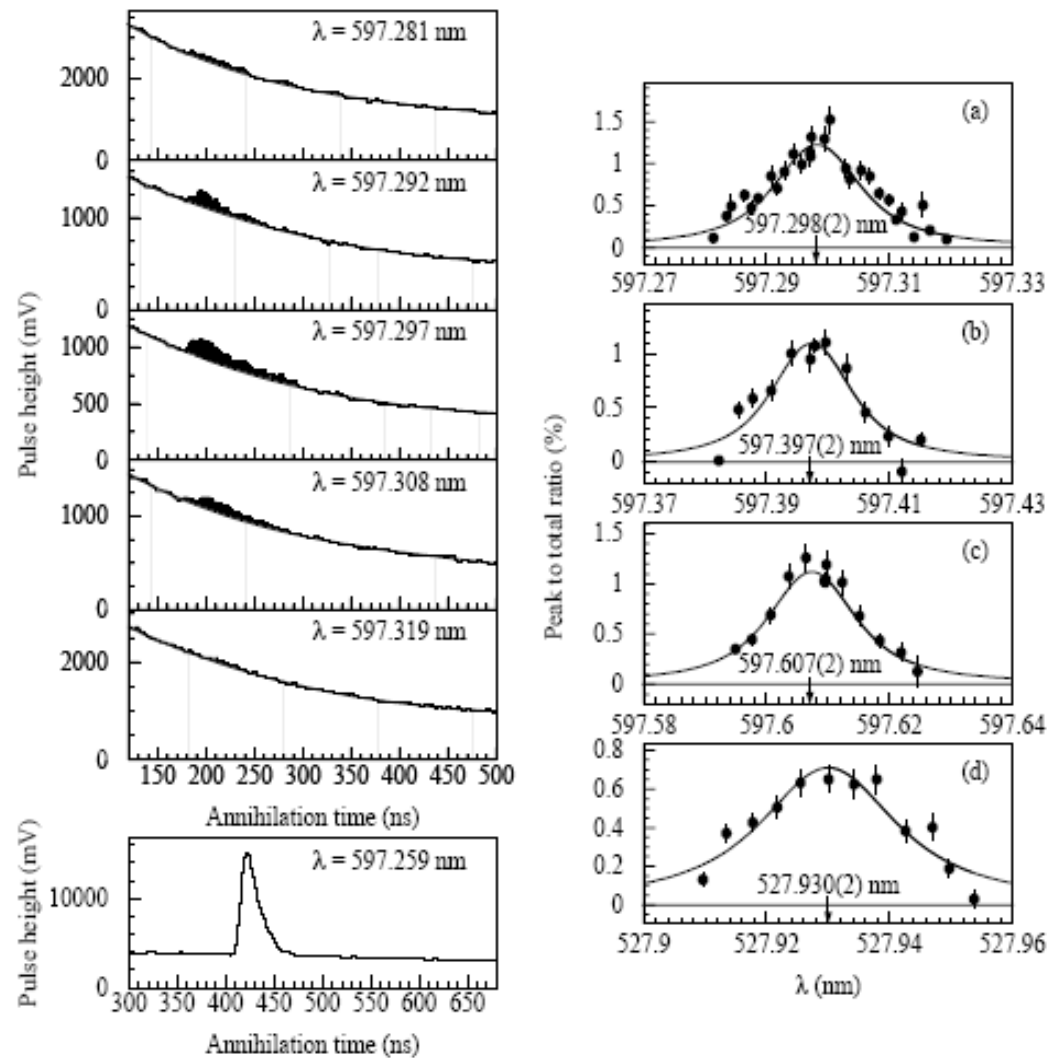
Fig. 54. Left: ADATS (photomultiplier output pulse shape recorded in a digital oscilloscope) obtained with laser irradiation at different wavelengths λ around 597.3 nm at 30 K and 5 bar with an H_2 admixture of 100 ppm. The small peak appearing as the laser wavelength approaches 597.297 nm indicates laser induced annihilations almost simultaneously with the laser firing time ($\sim$180 ns). For comparison, the lowest panel shows the resonance spike of a 'conventional' laser transition $[(n, l) = (39, 35) \rightarrow (38, 34)]$ from a metastable to a short-lived state in pure helium. Right: Resonance profiles for those transitions where wavelength scans were performed: (a) $(38, 35) \rightarrow (39, 36)$, (b) $(38, 36) \rightarrow (39, 37)$, (c) $(38, 37) \rightarrow (39, 38)$ and (d) $(37, 36) \rightarrow (38, 37)$. The central wavelengths obtained by fitting a convolution of a Gaussian function with a Lorentzian to the data are also shown. From [41].
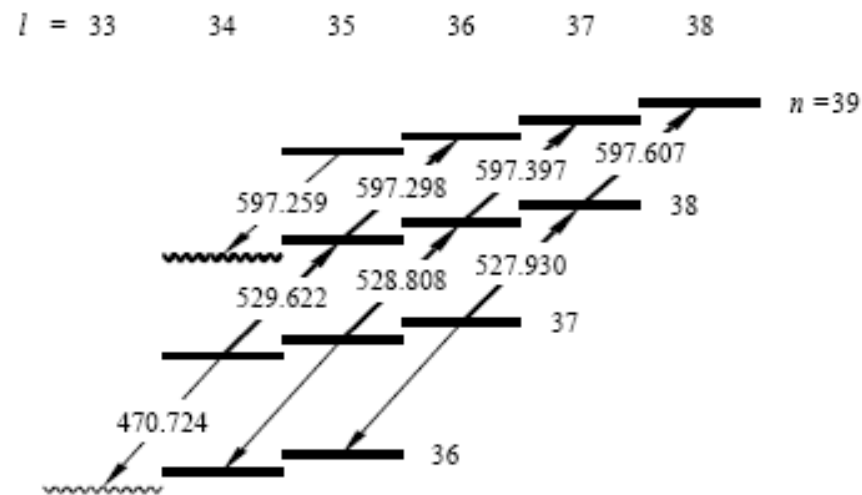
And many others

Fig. 55. Partial level scheme of $\bar{p}He^+$, summarizing the six transitions between normally metastable states observed by the new HAIR method (bold arrows). Only the vacuum wavelengths for transitions observed until now are shown (in units of nm). From [42].
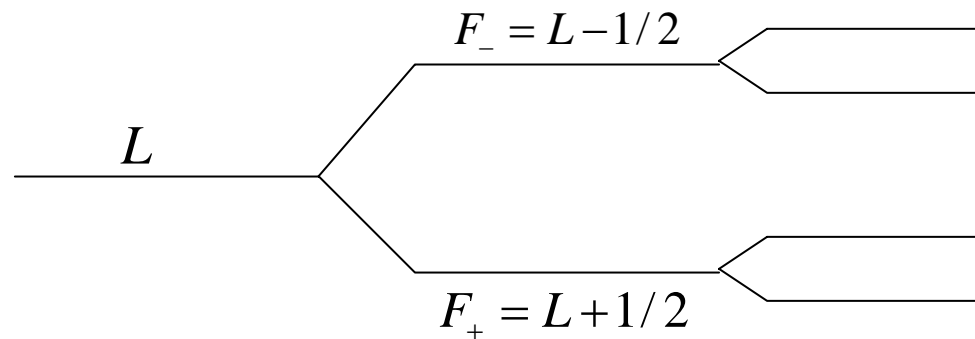
- **Fine- and hyperfine splitting**

Apart from the angular momentum L (mainly carried by the antiproton) there are two spins in the system: $\vec{S}_e$ and $\vec{S}_{\bar{p}}$

$$\vec{F} = \vec{L} + \vec{s}_e$$
$$\vec{J} = \vec{F} + \vec{s}_{\bar{p}}$$

Due to the magnetic moments the Hamiltonian contains $\vec{L} \cdot \vec{s}_e$ and $\vec{L} \cdot \vec{s}_{\bar{p}}$ type terms
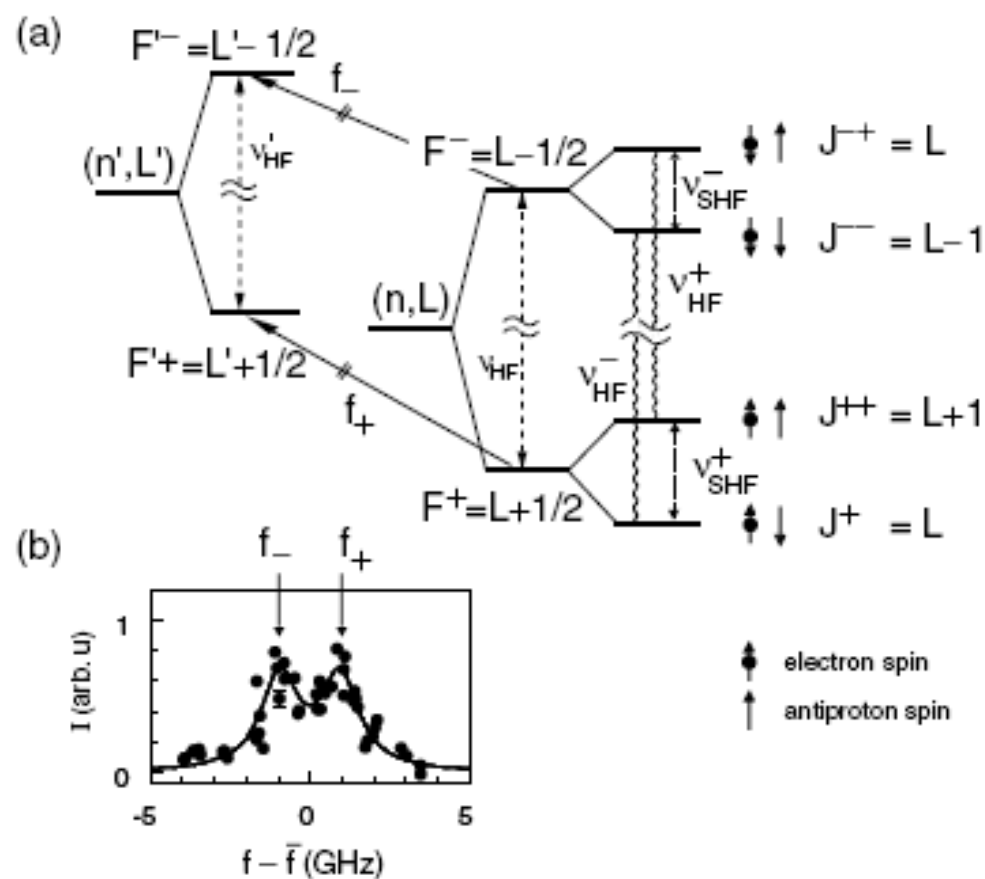The first one leads to a larger splitting (F+,F-) and the second one causes a further splitting

FIG. 1. (a) Schematic view of the splitting of a $\overline{p}\mathrm{He}^+$ state and observable laser transitions from the $F^\pm$ levels of a (n, L) state to a daughter state (n', L') (arrows). Wavy lines denote allowed magnetic transitions associated with an electron spin flip. (b) Laser scan of the 726.1 nm transition with $(n, L) = (37, 35)$ and $(n', L') = (38, 34)$ performed at the AD $[\overline{f} = (f_+ + f_-)/2]$.

How about the small splittings?
Two laser shots
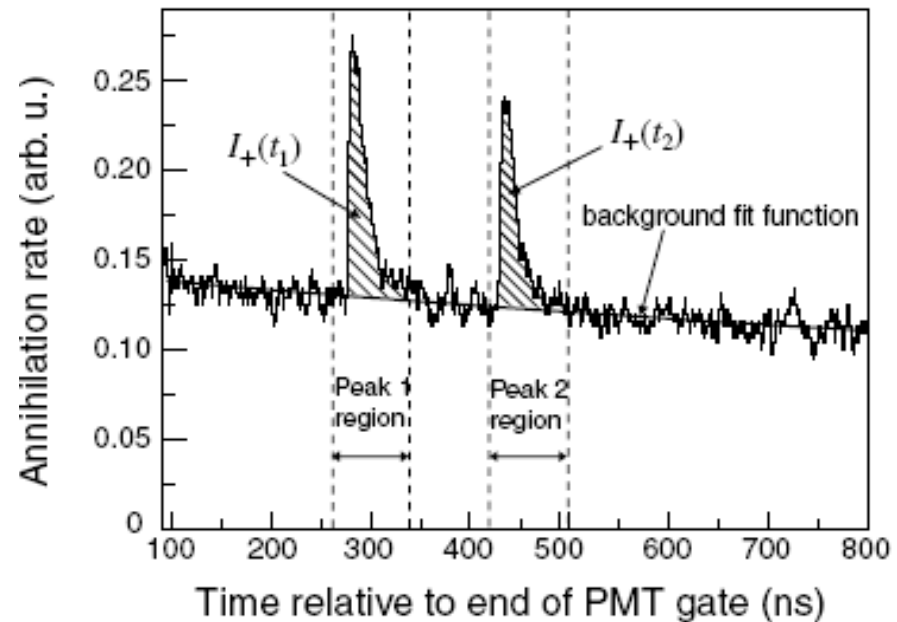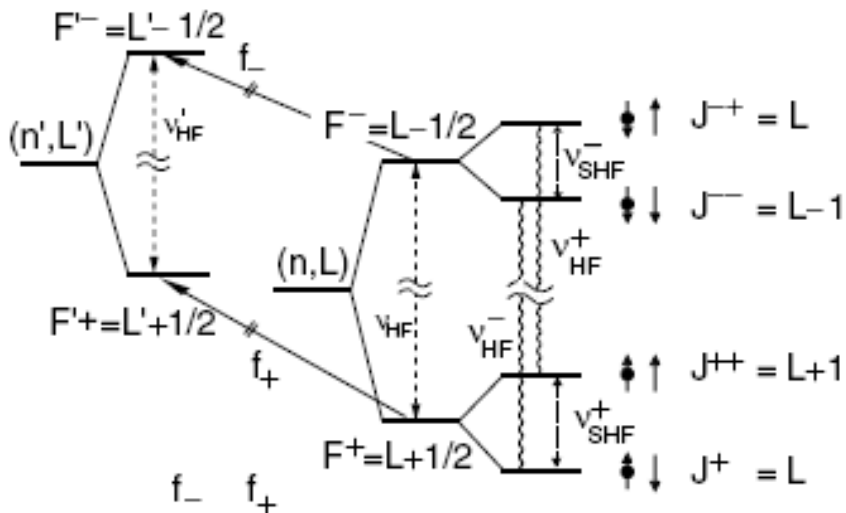
The laser-microwave-laser resonance method utilizes the following sequence: (i) a laser pulse tuned to one of the doublet lines [e.g., f_+ in Fig. 1(a)] preferentially depopulates the F_+ over the F_- doublet. (ii) The microwave pulse is applied; if it is resonant with either ν_{HF+} or ν_{HF-}, it transfers population from the F_- to the F_+ doublet. (iii) A second laser pulse at frequency f_+ measures the new population of F_+ after the microwave pulse.
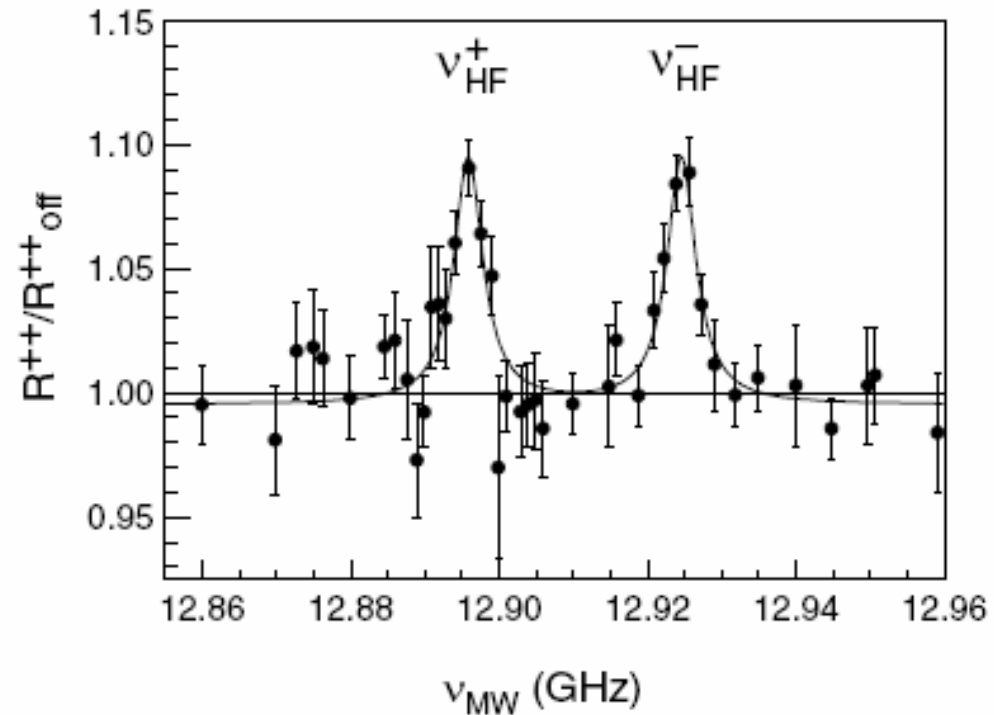
$I_+(t_2)/I_+(t_1)$ against ν_{mw}

FIG. 4. Average of all microwave scans showing clearly two resonance lines as predicted. The width of the lines of ~5 MHz corresponds to 4×10^{-4} of the central frequency.

Beautiful !!!

The precise calculation of these splittings involve spins, magnetic moments, relativistic corrections, and thus they become a probes of fundamental constants $m_{\bar{p}}, \mu_{\bar{p}}$, CPT theorem etc.

Auger emission probabilities

$$\Psi_{Jv} \sim \Psi_{Jv}^{B} + \Phi_{channel}$$

$$\Phi_{channel} = \sum_{NL} \phi_{NL}(\vec{R}) \varphi_{l}^{NL}(\vec{r})$$

$\Phi_{channel}$ describes the electron emission and its existence makes Ψ to be a resonance or Ψ_{Jv}^{B} "acquires" a width Γ. Different ways of calculating this width:

(a) Fermi "golden rule"

$$\Gamma = 2\pi \; \rho(E) \left\langle \Psi_{f} \mid H - E_{B} \mid \Psi_{Jv}^{B} \right\rangle$$

Here one have to guess the electron outgoing function

(b) Electron outgoing function of fixed form with unknown amplitude constant determined from Kohn variational principle

(c) From

$$\int \phi_{NL}(\vec{R})(E - H)\Psi_{Jv}(\vec{R}, \vec{r})d\vec{R} = 0$$

differential equations for $\varphi(r)$ to be solved with outgoing boundary conditions

(d) Complex rotation or scaling

$$r \rightarrow r' = r \cdot e^{i\theta} \qquad \frac{d}{dr} \rightarrow e^{i\theta} \cdot \frac{d}{dr'}$$
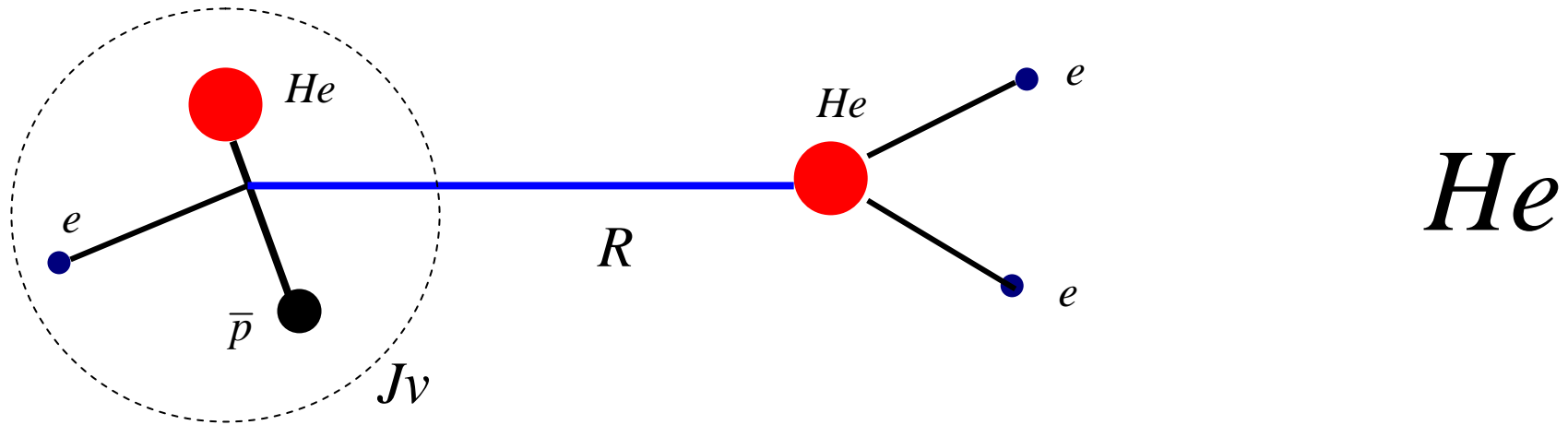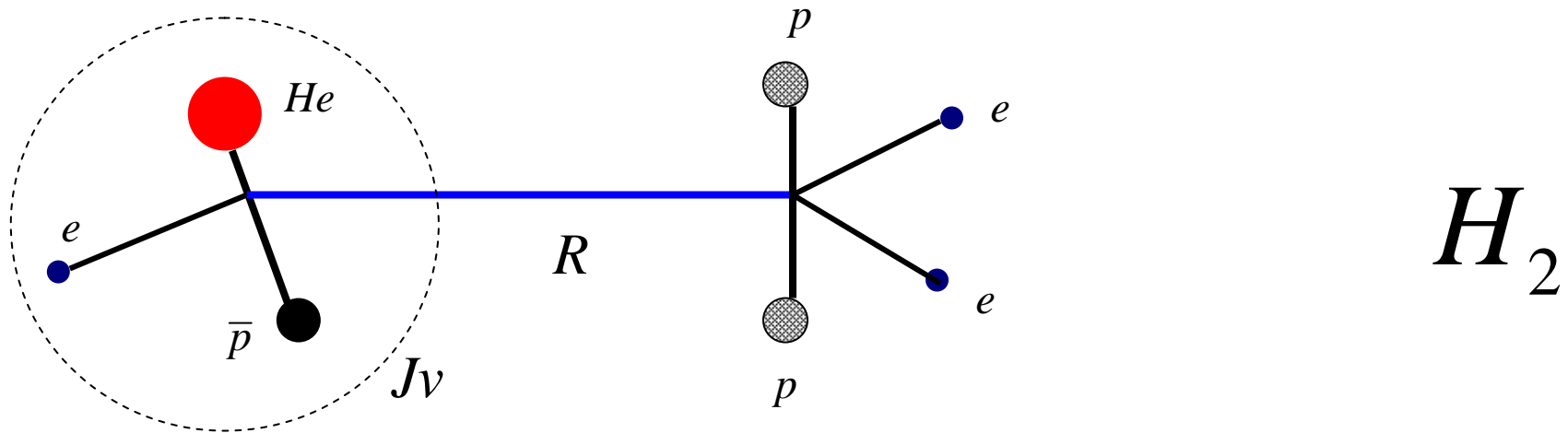
and

$$H(\theta)\Psi_\theta = E_\theta \Psi_\theta$$

and bound state methods can be applied to find the eigenvalues of $H(\theta)$ and the resonances appear as a discrete eigenvalues of $H(\theta)$. For this approach the Korobov-2 and the Kino-Kamimura wave functions are suitable – it is easy to rotate the exponentials.

Summarizing: with these approaches the observed Auger widths (you remember – the slope of the laser peaks) and the calculated ones are in acceptable agreement.

Interaction with media atoms and molecules